Implementation of a Novel OCDMA PON Based on Self-Heterodyne Filtering

Omri Levy, Avishay Alfandary, Yaniv Maroz, Gilad Katz, and Dan Sadot

***Abstract*—We propose a novel architecture of an optical code division multiple access, implemented by the method of self-heterodyne filtering (SHF). Theoretical and experimental results are introduced. The SHF method allows multiple channel access by the use of low-cost passive optical components, and standard on–off keying modulation.**

***Index Terms*—Optical code-division multiple access (OCDMA), passive optical networks (PON), self-heterodyne filtering, self-heterodyne detection, Mach–Zender interferometer (MZI), wavelength meetings.**

I. Introduction

OVER the recent years, wideband communication services have accelerated the deployment of local area networks (LANs) and in particular of fiber to the home application. These networks are characterized by high capacity, a large number of users, and require low costs of deployment and maintenance. A common solution is using passive optical networks (PONs) which are based on low-cost components.

Maximization of the network capacity is achieved by an efficient multiplexing of users. The most common methods of multiplexing are time or wavelength-division multiplexing (TDM/WDM). Optical code-division multiple access (OCDMA) was recently suggested as an alternative solution [1]. The main advantage of OCDMA systems is the lack of synchronization protocol requirement as in time-division multiple access (TDMA), and the lack of WDM narrow optical filtering and laser wavelength stabilization requirement as in WDM.

Here, we introduce theoretical analysis and experimental results of a fully implemented novel asynchronous OCDMA system, allowing multiple access by the use of self-heterodyne filtering (SHF) [2]. The system enables an additional multiplexing factor on top of existing optical networks. The system's architecture is presented in Fig. 1. Encoding/decoding is done using an unbalanced Mach–Zender Interferometer (MZI). Distinguishing between channels is achieved by using a unique time delay (fiber length) typical to each channel [2].

The main advantage of the SHF based system in comparison to other OCDMA systems is the use of standard low cost components at the end units, and the use of passive encoders/decoders.

Manuscript received August 01, 2008; revised January 23, 2009. Current version published July 15, 2009.

The authors are with the Electrical and Computer Engineering Department, Ben Gurion University of the Negev, Beer Sheva 84105, Israel

Color versions of one or more of the figures in this paper are available online at http://ieeexplore.ieee.org.

Digital Object Identifier 10.1109/JLT.2009.2017036

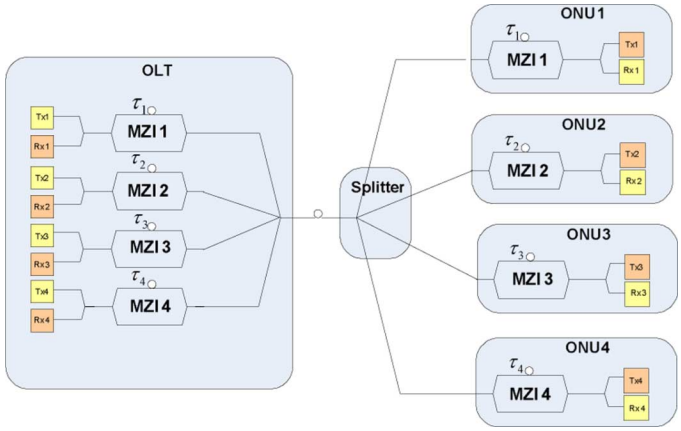

Fig. 1. SHF system's architecture.

The theory of the suggested method is discussed in Section II. A full implementation of a four asynchronous channel system running at a data rate of 1.25 Gbps over a distance of 25 km is presented in Section III.

II. Theory

The proposed system is based on the method described in [2], which was implemented using costly tunable laser and wavelength shift keying (WSK) modulation, while in the following proposed system, the transmitter is a standard off-the-shelf DFB laser, which is on–off keying (OOK) modulated.

A direct modulation of a DFB laser [3] produces an optical field which is AM–FM modulated [4]

$$e(t) = A(t) \cdot \exp\left(2\pi\nu t + 2\pi \int_t f(x)dx + \varphi\right) \quad (1)$$

where $A(t)$ is the optical field amplitude. ν is the optical carrier frequency, $f(x)$ is the instantaneous frequency deviation that is directly related to the output via the chirp phenomenon, and φ is the field phase.

In each MZI the optical input fields are divided into two paths, by a standard 3-dB coupler associated with the scattering matrix [5]

$$\frac{1}{\sqrt{2}}\begin{bmatrix} 1 & e^{j\frac{\pi}{2}} \\ e^{j\frac{\pi}{2}} & 1 \end{bmatrix} \quad (2)$$

A. Self-Heterodyne Filtering (Rejection) and Self-Homodyne Detection

Rejection of interferers is based on the SHF technique, while the detection of the desired channel is based on the self-homodyne detection (SHD) technique. Fig. 2 illustrates a scheme of

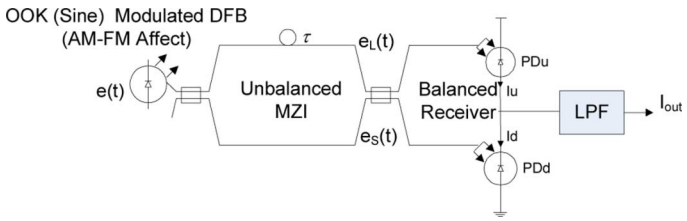

Fig. 2. Single MZI model.

a directly OOK modulated DFB laser, an unbalanced MZI with a delay difference of τ between its two arms, and a balanced receiver (BR) [5] followed by an electronic low-pass filter (LPF).

The optical output field of the laser is defined by (1). The fields at the inputs of the BR are $e_S(t)$ and $e_L(t)$ which travel through the short and the long arms of the MZI, respectively. Using (1) and (2) $e_S(t)$ and $e_L(t)$ are given by

$$\begin{aligned} e_S(t) &= \frac{1}{\sqrt{2}} A_S(t) \\ &\quad \cdot \exp\left[j\left(2\pi\nu t + 2\pi \int_t f_S(x)dx + \varphi_S \right) \right] \\ e_L(t) &= e_S(t-\tau)\cdot e^{j(\pi/2-\Delta\varphi)} \\ &= \frac{1}{\sqrt{2}} A_L(t) \\ &\quad \cdot \exp\left[j\left(2\pi\nu t + 2\pi \int_t f_L(x)dx + \varphi_L + \pi/2 \right) \right] \end{aligned} \tag{3}$$

where $A_s(t), f_s(t), \varphi_s$ and $A_L(t), f_L(t), \varphi_L$ are the optical amplitude, the instantaneous frequency deviation, and the phase of the fields of the short and the long arms of the MZI, respectively. $\Delta\varphi = \varphi_s - \varphi_L$.

According to [5] the output currents at each photodiode are

$$\begin{aligned} I_u(t) &= 0.25\Re \cdot |e_s(t) + e_L(t)\cdot e^{j\pi/2}|^2 \\ I_d(t) &= 0.25\Re \cdot |e_s(t)\cdot e^{j\pi/2} + e_L(t)|^2 \end{aligned} \tag{4}$$

where $\Re$ is the photodiode responsivity divided by twice the medium impedance. $I_u(t)$ and $I_d(t)$ are the output currents for the upper and lower arm diodes, respectively. The total output current $i_{\text{out}}(t)$ of the BR after the LPF is

$$\begin{aligned} i_{\text{out}}(t) &= \text{LPF}\{I_u(t) - I_d(t)\} \\ i_{\text{out}}(t) &= \text{LPF}\left\{ -\Re A_s(t) A_L(t) \right. \\ &\quad \left. \times \cos\left(2\pi \int_t f_{\text{if}}(x)dx + \Delta\phi \right) \right\} \end{aligned} \tag{5}$$

where $f_{\text{if}}(t) = f_L(t) - f_S(t)$ represents the instantaneous frequency difference between the fields at the long and short arms, and LPF$\{\}$ is the low-pass filtering operator. As long as $f_{\text{if}}(t)$ is higher than the LPF cutoff frequency, the signal is filtered out. This filtering method is the SHF. A simulation example of the SHF is presented in Fig. 3.

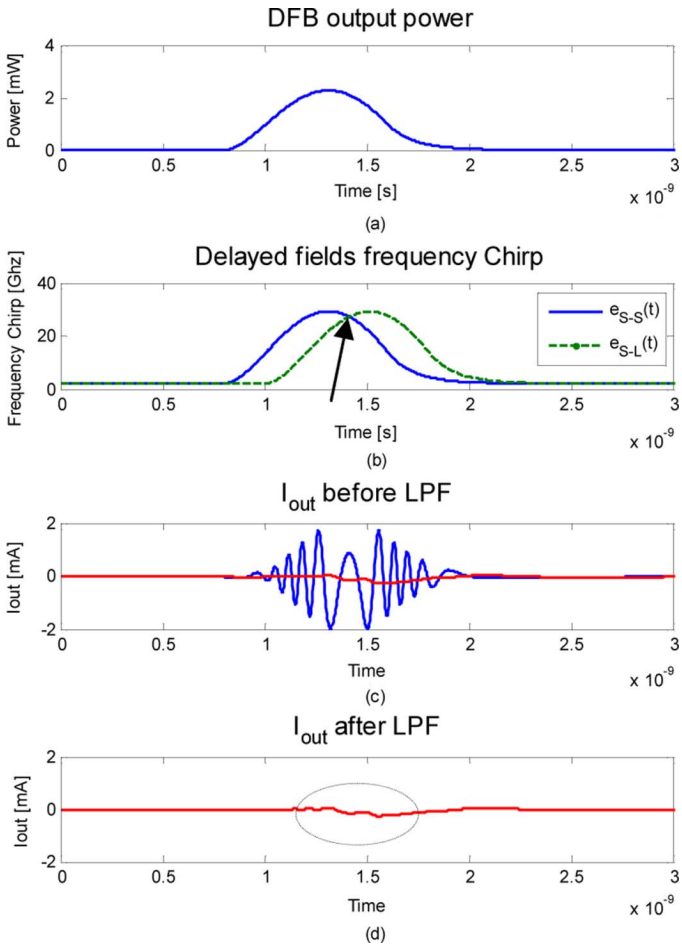

Fig. 3. Self-heterodyne filtering. (a) Typical modulated DFB output power. (b) Delayed fields with frequency chirp. (c) The output current of the PD. (d) The output current following LPF.

Fig. 3(a) presents the transmitter bit shape as a function of optical power. The transmitted information is the bit sequence: "010." Fig. 3(b) presents the instantaneous frequencies of the received fields $e_S(t)$ and $e_L(t)$. The arrow displayed in Fig. 3(b) indicates a short time interval in which the wavelengths of both fields are equal, $f_{\text{if}}(t)$ is relatively low, thus the signal is not filtered out by the LPF, resulting in ineffective SHF. The regions of interferences are called wavelength meetings (WMs). Fig. 3(c) presents the output current of the BR before electronic filtering. The output current frequency is constantly changing due to changes in $f_{\text{if}}(t)$, and mostly consists of high-frequency components, which, in turn, are filtered out by the electronic LPF, as shown in Fig. 3(d).

It is interesting to note that a sequence of consecutive "1"s results in a stabilized high power level and stabilized frequency level, leading to $f_{\text{if}}(t) = 0$. In such a case, the signal is not filtered out. The use of a sine modulation wave form, which is essentially a return to zero (RZ) shape, keeps the frequency alternating, thus enables the SHF regardless of the bit stream values.

Let us consider the case in which the MZI is in fact balanced, and $\tau = 0$. This case will result in SHD. The amplitudes and frequencies of both fields $e_S(t)$ and $e_L(t)$ will be the same, and $f_{\text{if}}(t) = 0$ for any given time. Using an LPF with a cutoff frequency high enough (higher than the information bandwidth),

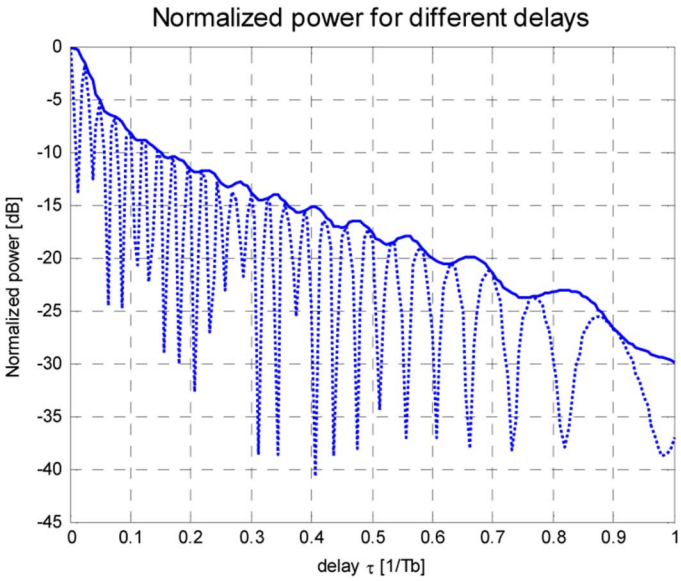

Fig. 4. Received bit power versus the unbalanced MZI delay difference.

the output current will be proportional to the transmitted power $(P(t))$

$$i_{\text{out}}(t) = \text{LPF}\left\{-\Re A(t)^2 \cos\left(2\pi \int_t 0dx + \Delta\varphi\right)\right\} = -\Re A(t)^2 \cos\Delta\varphi \underset{\Delta\varphi\to\pi}{\to} \propto P(t). \quad (6)$$

By using a phase stabilization mechanism in the MZI arms which keeps $\Delta\varphi = \pi$, (6) reduces to

$$I_{\text{out}} = -\Re A^2(t). \quad (7)$$

The stabilization may be done by a phase control mechanism which compensates for thermal effects.

According to (5), the output current decreases as $f_{\text{if}}(t)$ increases, while $f_{\text{if}}(t)$ is directly related to the optical delay, as described in (17) in the Appendix. Therefore, there is a direct relationship between the rejection efficiency to the optical delay. Computer simulation was used in order to measure the signal rejection efficiency of the SHF filtering (undesired channel rejection). The rejection efficiency is evaluated by measuring the power of the signal at the system's output [Fig. 3(d)]. The simulation results are depicted in Fig. 4.

The parameters used in the simulation of Fig. 4 are: bit rate of 1.25 Gbps, maximal chirp of 30 GHz, and a RZ (sine) bit shape. It is noticeable that the bit power is reduced as the time delay between the fields increases.

The dashed line represents the results for a constant phase $\Delta\varphi = \pi$ (5), while the envelope line represents the upper bound power.

B. Channel Coding

In order to apply channel coding, the principals of SHF and SHD that were described above for a single MZI configuration are extended to a double cascaded MZI scheme as described in Fig. 5. The first MZI forms the transmitter encoder while the second MZI forms the receiver decoder.

The signal is detected by a BR. e_u and e_d are the total fields incident on its upper and lower arm respectively and are defined by

$$\begin{aligned} e_u(t) &= e_{S-L}(t) + e_{L-L}(t) + e_{S-S}(t) + e_{L-S}(t) \\ e_d(t) &= e_{S-L}(t)\cdot e^{j\pi/2} + e_{L-L}(t)\cdot e^{j\pi/2} \\ &\quad + e_{S-S}(t)\cdot e^{-j\pi/2} + e_{L-S}(t)\cdot e^{-j\pi/2}. \end{aligned} \quad (8)$$

The indices S/L indicate the optical path short/long, respectively. The four fields have typical delays associated with the optical path, and a phase depending on the passes through the optical couplers, as described in [2]

$$\begin{aligned} e_{S-L}(t) &= 1/4\cdot e(t-\tau_{\text{de}})\cdot e^{j(\varphi_{\text{de}}+\pi)} \\ e_{S-S}(t) &= 1/4\cdot e(t) \\ e_{L-L}(t) &= 1/4\cdot e(t-\tau_{\text{de}}-\tau_{\text{en}})\cdot e^{j(\varphi_{\text{en}}+\varphi_{\text{de}})} \\ e_{L-S}(t) &= 1/4\cdot e(t-\tau_{\text{en}})\cdot e^{j(\varphi_{\text{en}}+\pi)} \end{aligned} \quad (9)$$

where τ_{en} and τ_{de} are the delays of the encoder and the decoder MZIs, respectively. φ_{en} and φ_{de} are random relative phases that are added to the fields traveling through the longer arms of the MZIs, due to inaccuracy of the fibers lengths.

The current at the receiver output after low-pass filtering is shown in (10) at the bottom of the page.

In order to apply correct decoding at the receiver's end the delay differences of both MZIs should be identical: $\tau_{\text{en}} = \tau_{\text{de}} = \tau$. Fig. 6 illustrates the fields' temporal frequencies at the receiver's input.

The fields $e_{S-L}(t)$ and $e_{L-S}(t)$ propagate through a similar optical path and have similar temporal frequencies, therefore SHD is performed. All the other fields' pairs propagate through different optical paths, and therefore are filtered out by the SHF principal, while WMs occur. The output current at the BR output is given by (11), shown at the bottom of the next page [5].

The latter expression reveals that the output current is proportional to the optical power after modulation and therefore the data is detected. As described in (6), phase stabilization is necessary. It is also noticeable that only $1/4$ of the optical power is useful.

Fig. 7 illustrates the temporal frequencies of the four fields for the case of channel rejection where $\tau_{\text{en}} \neq \tau_{\text{de}}$.

In this case, a relative delay between the fields is obtained. As a result, the four elements in (9) will be filtered out due to the SHF principal. Even though most of the undesired channels are rejected, the WMs interfere with the correctly decoded channel and form multi-access interference (MAI) [1].

$$i_{\text{out}}(t) = \text{LPF}\left\{\Re\cdot 4\text{Re}\begin{bmatrix} e_{S-L}(t)\cdot e_{L-S}(t)^* + e_{S-L}(t)\cdot e_{S-S}(t)^* \\ +e_{L-L}(t)\cdot e_{S-S}(t)^* + e_{L-L}(t)\cdot e_{L-S}(t)^* \end{bmatrix}\right\} \quad (10)$$

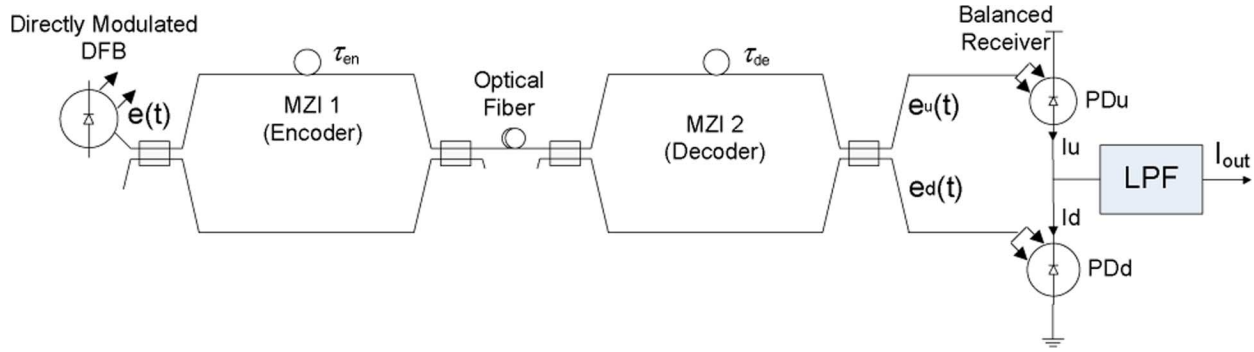

Fig. 5. Double cascaded MZI configuration.

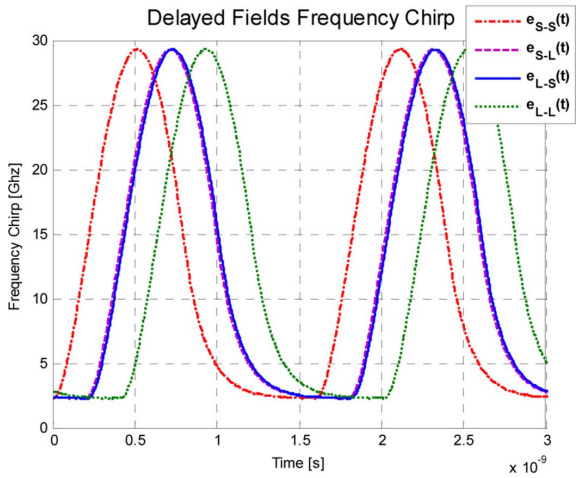

Fig. 6. Fields' frequencies for a desired channel.

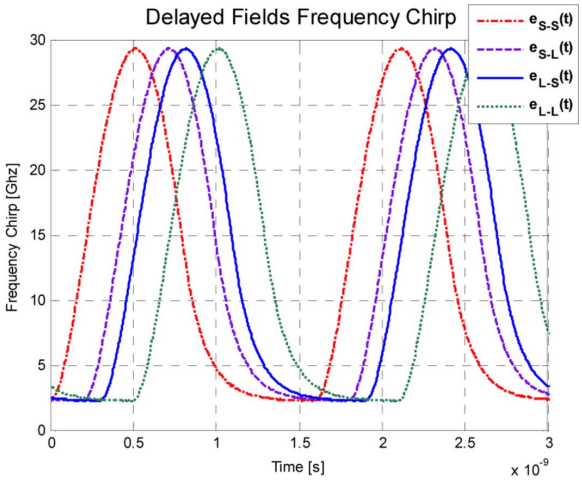

Fig. 7. Fields' frequencies for a rejected channel.

C. Four-Channel System

A four-channel system architecture is illustrated in Fig. 8, this architecture enables a simultaneous asynchronous transmission and reception of four different channels, multiplexed into a shared fiber. The channel code is defined by the channel's typical MZI arms length difference.

The output current at receiver j in an N channel system is given by (12), shown at the bottom of the next page, where $e_{S_i-L_j}(t)$ for an example is the field that propagates through the short arm of channel i and the long arm of channel j. The second part of the equation is mostly filtered out using the SHF; therefore, (12) is boiled down to an output current which is directly dependent on the data signal's amplitude and $\Delta\varphi$

$$\begin{aligned} i_{\text{out}}(t) &\approx 4\Re\text{Re}\left[e_{S_j-L_j}(t)\cdot e_{S_j-S_j}(t)\right] \\ &= -\frac{1}{4N^2}\Re\cdot\left[A(t)^2\cdot\cos(\Delta\varphi)\right] \end{aligned} \tag{13}$$

Phase stabilization ($\Delta\varphi=\pi$) maximizes the detected signal output

$$i_{\text{out}}(t) \approx \frac{1}{4N^2}\Re A(t)^2 \propto P(t). \tag{14}$$

The $1/N^2$ factor indicates that an optical amplifier may be needed at the optical line terminal (OLT) output for extended reach PON implementations.

III. System Implementation and Experimental Results

As a first step, in order to verify the feasibility of the SHF concept, the experimental setup illustrated in Fig. 9 was performed.

A standard transmitter optical subassembly (TOSA) DFB laser is directly modulated by a 1.25-Gbps pseudo random bit sequence (PRBS) followed by an electronic filter results in a sinusoidal bit shape. The modulation current is set to 120 $\text{mA}_{\text{pk-pk}}$ introducing a chirp of 30 GHz. The optical

$$\begin{aligned} i_{\text{out}}(t) &= 4\Re\cdot\left[e_{S-L}(t)\cdot e_{L-S}(t)^*\right]+\text{LPF}\left\{\Re\cdot 4\text{Re}\left[\begin{matrix} e_{S-L}(t)\cdot e_{S-S}(t)^* \\ +e_{L-L}(t)\cdot e_{S-S}(t)^*+e_{L-L}(t)\cdot e_{L-S}(t)^*\end{matrix}\right]\right\} \\ i_{\text{out}}(t) &= -\frac{1}{4}\Re\cdot\left[A(t)^2\cdot\cos(\Delta\varphi)\right]+\text{WMs}\underset{\Delta\varphi\to\pi}{\rightarrow} i_{\text{out}}(t)=\frac{1}{4}\Re A(t)^2+\text{WMs}\propto P(t) \end{aligned} \tag{11}$$

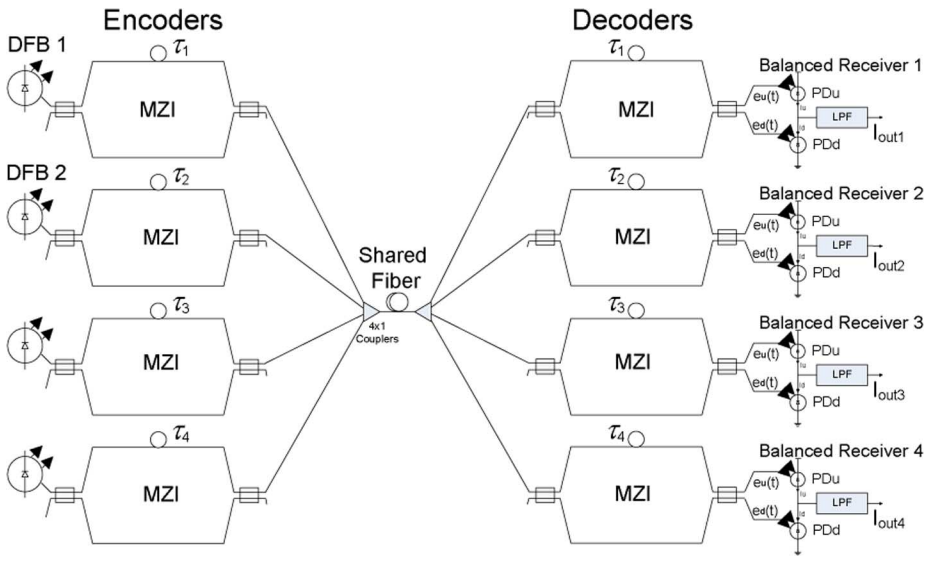

Fig. 8. Four-channel system architecture.

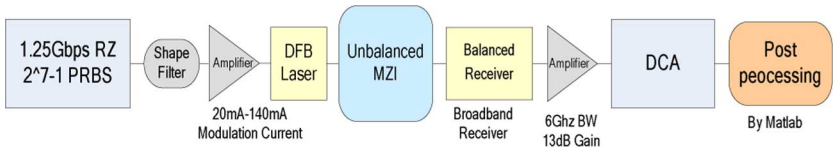

Fig. 9. Single MZI experiment setup.

signal propagates through one MZI with a variable arms difference. At the receiver end, the detection is performed by a broadband BR. The BR output current is amplified by 13 dB using an RF amplifier with a 6-GHz bandwidth, and sampled by a digital communication analyzer (DCA). Computer postprocessing is applied to perform digital low-pass filtering with a cutoff frequency of 1.25 GHz. An analog electronic LPF may replace the digital filter in practical implementations.

The signal rejection efficiency is evaluated by measuring the maximal signal value $V_{\mathrm{pk-pk}}$, versus MZI arms lengths difference. The experimental and computer simulation (same simulation as in Fig. 4) results are compared in Fig. 10. Very good agreement is observed between the theoretical prediction of SHF rejection [Fig. 3(d)] (continuous line) and actual measurements (crosses).

In the following, a complete system implementation was demonstrated, as described in Fig. 11.

Four TOSA DFB lasers are directly modulated by PRBS at a data rate of 1.25 Gbps. The bits have a sinusoidal shape. The modulation current is set to 120 $\mathrm{mA_{pk-pk}}$ introducing a chirp of 30 GHz. Each MZI has a unique time delay equivalent to the following arm length differences

$$\delta_1 = 9\,\mathrm{cm}, \quad \delta_2 = 10.8\,\mathrm{cm}, \quad \delta_3 = 12.7\,\mathrm{cm}, \quad \delta_4 = 14.5\,\mathrm{cm}.$$

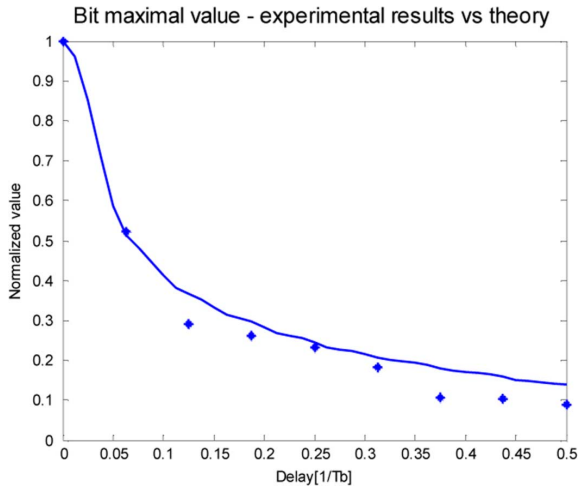

Fig. 10. Experimental and theoretical signal rejection measurements versus MZI arms lengths difference.

The delays are designed to minimize the number of WMs, and maximize the time duration between WMs. Further discussion on the fiber delay lengths design is detailed in the Appendix.

Delay lines are set at the outputs of the MZIs, in order to decorrelate the data which is generated by the same source.

$$i_{\mathrm{out}}(t) = 4\Re\mathrm{Re}\left[e_{S_j-L_j}(t)\cdot e_{S_j-S_j}(t)\right] + \mathrm{LPF}\left\{4\Re\mathrm{Re}\sum_{i=1}^{N}\begin{bmatrix} e_{S_i-L_j}(t)\cdot e_{S_i-S_j}(t) + e_{S_i-L_j}(t)\cdot e_{L_i-S_j}(t) + \\ e_{L_i-L_j}(t)\cdot e_{S_i-S_j}(t)^* + e_{L_i-L_j}(t)\cdot e_{L_i-S_j}(t)^* \end{bmatrix}\right\}, \quad i,j\in[1,N] \quad (12)$$

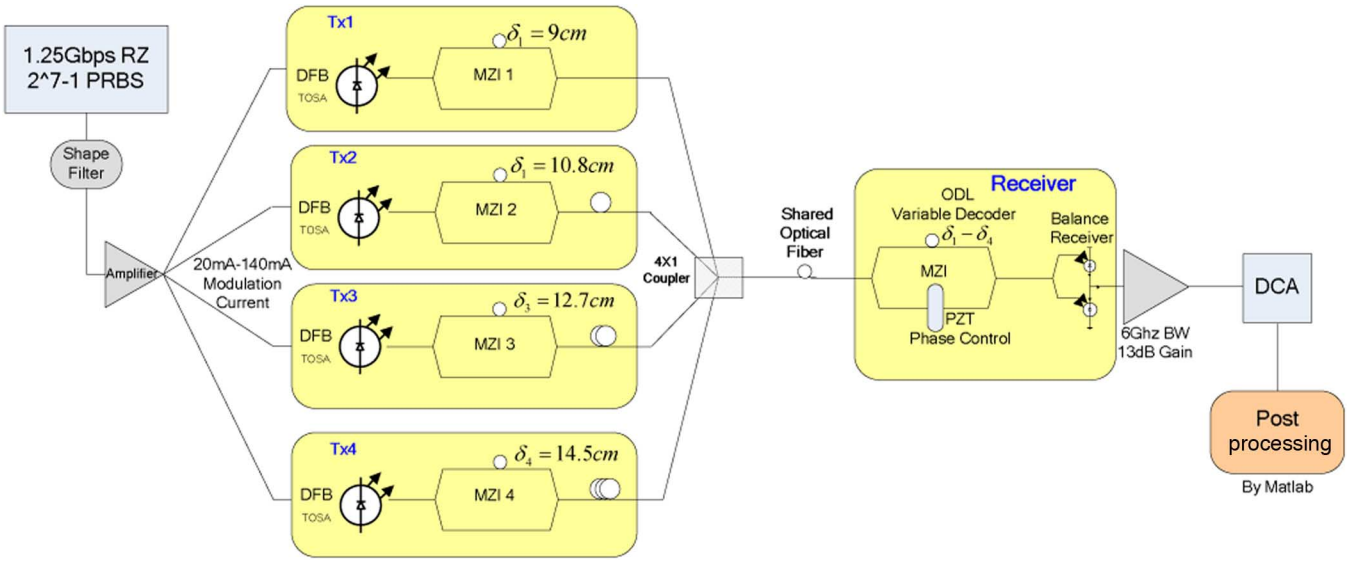

Fig. 11. Four-channel system experimental setup.

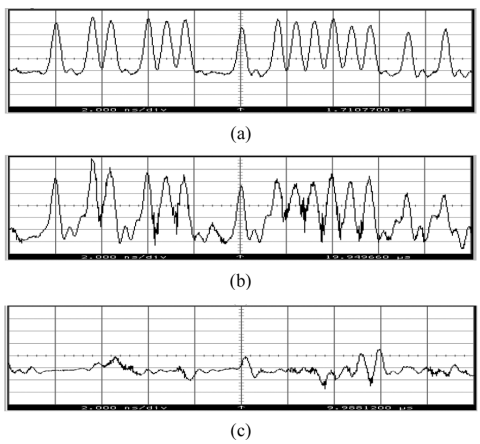

Fig. 12. Output signals in the time domain (2 ns/div). (a) Single user-information only. (b) Four active channels (three interferers and one information channel). (c) Three interfering channels only.

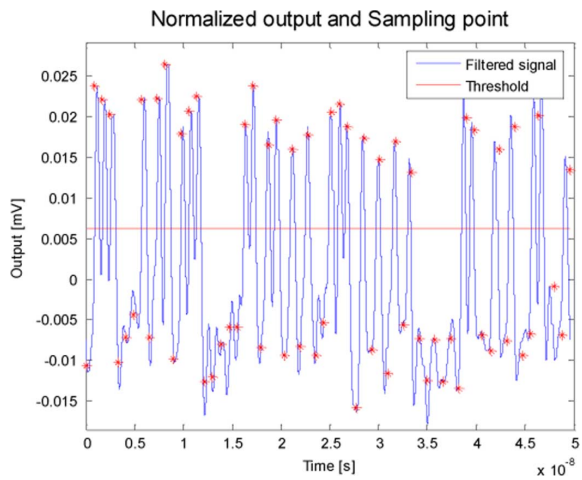

Fig. 13. Digital postprocessing of the detected channel.

The four encoded optical data streams are coupled into a shared optical fiber, by a standard 4X1 coupler. At the receiver's end, an MZI with a variable arms length difference decodes the data, enabling the reception of one out of the four channels at a time.

On one arm of the MZI, a phase control mechanism is placed, in order to overcome thermal effects and maintains $\Delta\varphi \approx \pi$. In production, MZI and its stabilization may be implemented using a thermoelectric cooler.

A BR with responsivity $\mathcal{R} = 0.5$ [A/W] is used to detect the signal. The BR output current is amplified and sampled by the same DCA. Fig. 12 presents the detected signal as observed by the DCA while one channel is active [Fig. 12(a)], all four channels (information and interferers) are active [Fig. 12(b)], and while only the three interfering channels are active [Fig. 12(c)]. All plots have the same X and Y scales.

Fig. 13 illustrates the outcome of post processing result that is applied at the receiver, while all of the channels are active, and channel 1 is detected. A digital low-pass filter with a cutoff frequency of 1.25 Gbps is used, and the signal is sampled at the optimal sampling point (crosses). In turn, a threshold for hard decision is determined. The corresponding eye-diagram of the detected channel is illustrated in Fig. 14.

Fig. 14 presents the received signal while high SNR is applied (received power $= -4$ dBm), therefore the main cause for the eye closure is the MAI from the three interferers. Since four channels are transmitting simultaneously, and each received bit is affected by the current bit and the previous one (due to the MZI delay), there is an 8-bit combination space, thus $2^8 = 256$ combinations at the receiver's end. This analysis represents the entire MAI combination space, and a set of measurements that consistently represent the MAI statistics was performed accordingly.

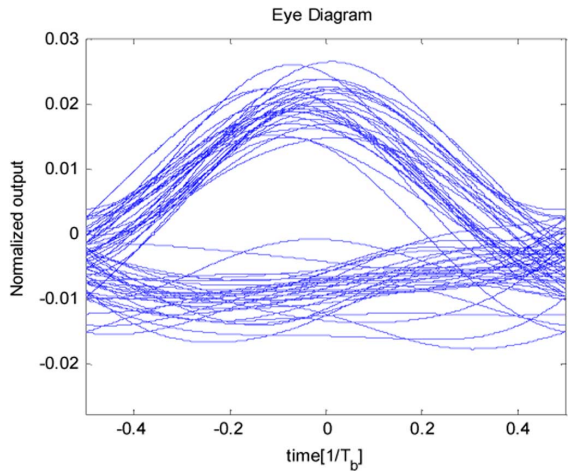

Fig. 14. Eye-diagram of the detected channel.

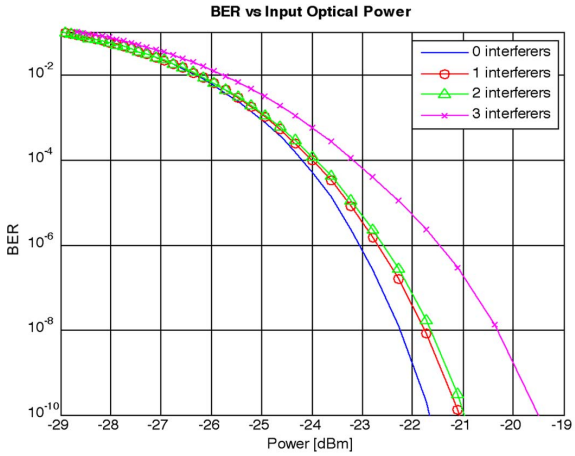

Fig. 15. BER estimations of channel 1.

Calculation of BER versus received optical power for various number of interferers is illustrated in Fig. 15. The calculations are based on the BER equation of normally distributed noise [7]

$$\mathrm{BER} = \frac{1}{N_1 \cdot N_0} \sum_{i=1}^{N_1} \sum_{j=1}^{N_0} Q\left(\frac{y_1^i - y_0^j}{2\sigma_n} \cdot \frac{1}{\mathrm{Att}} \right) \tag{15}$$

where N_0 and N_1 are the total number of "1"s and "0"s and y_1^i and y_0^j are the measured values (of the experiment) of binary "1" and "0," respectively (Fig. 13). Att represents the channel attenuation and σ_n is the referred input noise in RMS units taken as indicated by an off-the-shelf PD receiver that introduces a receiver sensitivity of -29 dBm $(\mathrm{BER} = 10^{-10})$ at 2.5 Gbps in a conventional OOK transmission link.

According to the results of Fig. 15, the receiver sensitivity of the SHF system is -23 dBm. The 6-dB power penalty is a consequence of inherent 3-dB loss of the SHF method, and an additional 3-dB loss due to the responsivity of the PDs (0.5 A/w instead of 0.9 A/w).

The multiple channel MAI in the four-channel system imposes additional 2 dB.

While increasing the fiber length to 25 km, the optical signal is chromatically dispersed, and additional 2 dB of power penalty

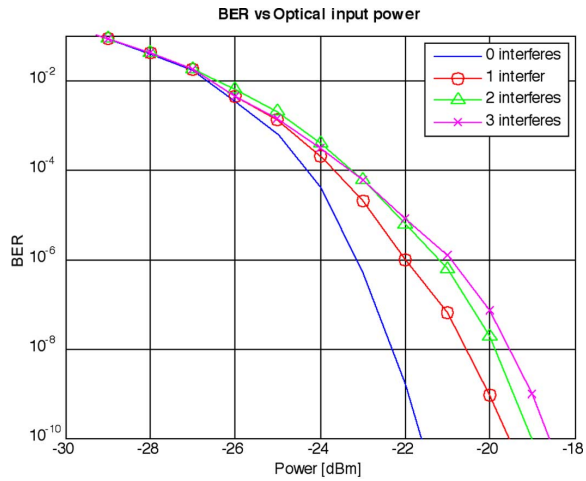

Fig. 16. BER estimations of the detected channel after 25 km.

is introduced. This additional dispersion penalty results from the large chirp (30 GHz) that was used for SHF enhancement. Fig. 16 illustrates the performance of the desired channel for the case of 25-km fiber.

IV. Summary

A full implementation of a novel OCDMA multiplexing scheme based on SHF is presented for the first time. Experimental results of a four-channel system demonstration are presented, indicating very good agreement with theoretical prediction. The demonstration includes four channels transmitting at a data rate of 1.25 Gbps, coupled into a shared 25-km fiber. BER results indicate a power penalty of 8 dB in comparison to serial transmission. The use of a BR instead of a single PD and the necessity of phase stabilization are the system cons.

It is experimentally demonstrated that the power penalty introduced by the interfering channels is relatively low (less than 2 dB). The described system enables the increase of PONs capacity by a factor of four on top of existing WDM and TDM multiplexing solutions, with the use of low cost off-the-shelf components.

Appendix
Maximal Number of Channels Allowed

The purpose of this Appendix is to present a detailed explanation of the theoretical design rule to determine the optical channel delays and the scalability of the SHF system.

The output signal in the case of correctly decoded signal consists of frequency components within the range of $[0, 2R_b]$. For the case of an interferer, the signal is modulated by a varying frequency carrier $f_{\mathrm{IF}}(t)$ according to (5).

In order to effectively filter the interferer without damaging the information, the signals should be spectrally separated. Considering the carrier frequency at its maximum, the condition of spectral separation will be

$$\max(f_{\mathrm{IF}}) = f_{\mathrm{IF\,max}} > 4R_b. \tag{16}$$

Let us denote $df_{\max}$ as the maximal frequency chirp of the optical field and τ as the relative delay between the fields. Using geometrical model the relations of the parameters are given by

$$\frac{df_{\max}}{f_{\mathrm{IF}\max}} = \frac{T_b/2}{\tau}. \tag{17}$$

Using (16) and (17), the condition that enables the SHF is given by

$$\tau_{\min} = \frac{2}{df_{\max}}. \tag{18}$$

The latter result implies that the minimal delay is affected only by the chirp effect and not by the bit rate.

The typical delay τ_i of each channel can be chosen out of two ranges specified in (19) and (20)

$$\tau_{\min} < \tau_i < \frac{1}{2}(T_b - \tau_{\min}) \tag{19}$$

$$\frac{1}{2}(T_b + \tau_{\min}) < \tau_i < (T_b - \tau_{\min}) \tag{20}$$

For the case of a multiple channel system, in order to minimize the MAI. The typical delays of the channels (Fig. 8) have to follow the condition:

$$|\tau_i - \tau_j| > \tau_{\min} \quad (i \neq j) \tag{21}$$

where $i, j \in [1, N]$ represent different channels. All The delays are picked from the same range [(19) or (20)].

The maximal number of channels is derived out of the above as

$$N_{\max} = \left\lfloor \left(\left(\frac{1}{2}(T_b - \tau_{\min}) \right) - \tau_{\min} \right) \Big/ \tau_{\min} \right\rfloor \tag{22}$$

Combining the last result with (18) gives

$$N_{\max} = \left\lfloor \frac{df_{\max}}{4Rb} - 1.5 \right\rfloor \tag{23}$$

For an example, in our experiment setup, described in Section III: $df_{\max} = 30$ GHz, $T_b = 800$ ps, $N = 4$.

Therefore, according to (18): $\tau_{\min} = 1.3\,\mathrm{cm}/v_g$, and $\delta_{\min} = \tau_{\min} v_g = 1.3$ cm, where $v_g = 2{\cdot}10^8$ (m/s) is the group velocity.

According to (20)

$$\frac{8.65\mathrm{cm}}{v_g} < \tau_i < \frac{14.7\mathrm{cm}}{v_g}$$

Equally spacing of the channels within the margin above and considering (21) provide the chosen channels delays

$$\delta_1 = 9\,\mathrm{cm}, \quad \delta_2 = 10.8\,\mathrm{cm},$$
$$\delta_3 = 12.7\,\mathrm{cm}, \quad \delta_4 = 14.5\,\mathrm{cm}$$

REFERENCES

[1] P. R. Prucnal, "Optical Code Division Multiple Access," 2006, pp. 1–55, 165–241.

[2] H. Joseph *et al.*, "A novel self-heterodyne filtering method by wavelength shift keying modulation for optical CDMA," *IEEE Photon. Technol. Lett.*, vol. 17, no. 6, pp. 1346–1348, Jun. 2005.

[3] E. Buimovich and D. Sadot, "Inclusive study of the effect of thermal chirp on interferometric homodyne crosstalk induced penalty in directly modulated DFB laser communication systems," *J. Lightw. Technol.*, vol. 23, no. 9, pp. 2662–2672, Sep. 2005.

[4] G. P. Agrawal, *Semiconductor Lasers*. New York: Van Nostrand Reinhold, 1993.

[5] L. Kazovsky, *Optical Fiber Communication Systems*. Boston, MA: Artech House, 1996, pp. 294–298.

[6] G. P. Agrawal, *Fiber Optic Communication Systems*. New York: Wiley.

[7] J. G. Proakis, *Digital Communication*. New York: McGraw-Hill, 1995, pp. 257–260.

Omri Levy, photograph and biography not available at the time of publication.

Avishay Alfandary, photograph and biography not available at the time of publication.

Yaniv Maroz, photograph and biography not available at the time of publication.

Gilad Katz, photograph and biography not available at the time of publication.

Dan Sadot received the B.Sc., M.Sc., and Ph.D. degrees *(summa cum laude)* from the Ben Gurion University of the Negev, Beer Sheva, Israel, in 1988, 1990, and 1994, respectively, all in electrical and computer engineering.

From 1994 to 1995, he was a Postdoctorate Associate in the Optical Communication Research Laboratory, Department of Electrical Engineering, Stanford University, Stanford, CA. His Ph.D. studies were supported by the Clore scholarship, and his post-doctorate was supported by both the Fulbright and the Rothchild scholarships. At Stanford University, he was involved in the STARNET broadband coherent optical network project. In 1995, he joined Ben Gurion University in the Electrical and Computer Engineering Department as a Senior Lecturer, and in 2001 he was appointed as an Associate Professor, where he is leading a new research program in optical fiber communications. During 2000–2001, he was appointed to be the Department Head of communications systems engineering at Ben Gurion University. His current activities include dynamic WDM networks, tunable lasers and filters, optical burst/packet switching, optical CDMA, passive optical networks (PONs), and electronic compensation schemes for impairments in optical fiber communications. He is Chairman of the Electrical and Computer Engineering Department, and Vice Dean of the Faculty of Engineering Science.

Prof. Sadot was appointed to be the founder and chair of the IEEE Photonics society (formerly IEEE LEOS) chapter in Israel in 1996.